Nature of the Mott Transition in Ca_2RuO_4

E. Gorelov,[1] M. Karolak,[2] T. O. Wehling,[2] F. Lechermann,[2] A. I. Lichtenstein,[2] and E. Pavarini[1]

[1]*Institut für Festkörperforschung and Institute for Advanced Simulation, Forschungszentrum Jülich, 52425 Jülich, Germany*
[2]*I. Institut für Theoretische Physik, Universität Hamburg, Jungiusstraße 9, D-20355 Hamburg, Germany*

We study the origin of the temperature-induced Mott transition in Ca_2RuO_4. As a method we use the local-density approximation + dynamical mean-field theory. We show the following. (i) The Mott transition is driven by the change in structure from long to short **c**-axis layered perovskite (L-$Pbca \rightarrow S$-$Pbca$); it occurs together with orbital order, which follows, rather than produces, the structural transition. (ii) In the metallic L-$Pbca$ phase the orbital polarization is ~ 0. (iii) In the insulating S-$Pbca$ phase the lower energy orbital, $\sim xy$, is full. (iv) The spin-flip and pair-hopping Coulomb terms reduce the effective masses in the metallic phase. Our results indicate that a similar scenario applies to $Ca_{2-x}Sr_xRuO_4$ ($x \leq 0.2$). In the metallic $x \leq 0.5$ structures electrons are progressively transferred to the xz/yz bands with increasing x; however, we find no orbital-selective Mott transition down to ~ 300 K.

The layered perovskite Ca_2RuO_4 (Ru $4d^4$, $t_{2g}^4 e_g^0$) undergoes a paramagnetic metal-paramagnetic insulator transition (MIT) at $T_{MIT} \sim 360$ K [1]. A similar insulator-to-metal transition happens also by application of a modest (~ 0.5 GPa) pressure [2] and finally when Ca is partially substituted by Sr ($Ca_{2-x}Sr_xRuO_4$, $x \leq 0.2$) [3,4]. The nature of these transitions, in particular across $x = 0.2$, has been debated for a decade [5–13]. While it is clear that a Mott-type mechanism makes the 2/3-filled t_{2g} bands insulating, two opposite scenarios, with different orbital occupations $n = (n_{xy}, n_{xz} + n_{yz})$ and polarizations $p \equiv n_{xy} - (n_{xz} + n_{yz})/2$, have been suggested. In the first, only the xy band becomes metallic; i.e., the transition is orbital selective (OSMT) [5]; n and p jump from (2, 2) and 1 in the insulator to (1, 3) and $-1/2$ in the metal. In the second, there is a single Mott transition, assisted by the crystal-field splitting $\Delta = \epsilon_{xz/yz} - \epsilon_{xy} > 0$ [13], similar to the case of $3d^1$ perovskites [14]; $p > 0$ in all phases. To date the issue remains open. Recently, for $x = 0.2$ a novel (xy insulating, $n_{xy} = 1.5$ and $p = 1/4$) OSMT was inferred from angle-resolved photoemission (ARPES) experiments [7], but other ARPES data show three metallic bands and no OSMT [8].

Ca_2RuO_4 is made of RuO_2 layers built up of corner-sharing RuO_6 octhahedra (space group $Pbca$ [3,15]). This structure (Fig. 1) combines a rotation of the octahedra around the **c** axis with a tilt around the **b** axis. It is similar to that of the tetragonal unconventional superconductor Sr_2RuO_4; the corresponding pseudotetragonal axes **x**, **y**, and **z** are shown in Fig. 1. The structure of Ca_2RuO_4 is characterized by a long **c** axis (L-$Pbca$) above $T_S \sim 356$ K and by a short one (S-$Pbca$) below T_S. The L- and S-$Pbca$ phases are also observed in $Ca_{2-x}Sr_xRuO_4$ for all $x \leq 0.2$, but T_S decreases with increasing x; for $x > 0.2$ the system becomes tetragonal (for $x < 1.5$: $I41/acd$, **c**-axis rotations only).

Because of the layered structure, the $\sim xz, yz$ bandwidth, $W_{xz/yz}$, is about one-half of the $\sim xy$ bandwidth, W_{xy}. Because of the structural distortions, the t_{2g} manifold splits into nondegenerate crystal-field states. Many-body studies of 3-band Hubbard models show that a large difference in bandwidths, a crystal-field splitting Δ and a finite Coulomb exchange interaction can affect the nature of the Mott transition [5,13,16]. Simple models neglect, however, the actual effects of distortions on the electronic structure; such effects could be crucial [14] to the mechanism of the MIT. On the other hand, approximate treatments of the many-body effects [6], or the neglect of the spin-flip and pair-hopping contribution to the Coulomb exchange inter-
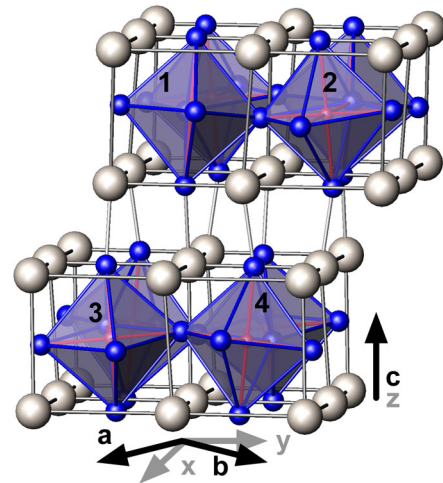

FIG. 1 (color online). Ca_2RuO_4 L-$Pbca$ [3,15]. The primitive cell is orthorhombic with 4 formula units; $\mathbf{x} \sim (\mathbf{a} + \mathbf{b})/2$, $\mathbf{y} \sim (\mathbf{b} - \mathbf{a})/2$, $\mathbf{z} = \mathbf{c}$ are the pseudotetragonal axes. Ru sites i at $\mathbf{T}_i$ ($i = 2, 3, 4$) are equivalent to site 1 at $\mathbf{T}_1$, with operations $\mathbf{a} \rightarrow -\mathbf{a}$ ($i = 2$), $\mathbf{c} \rightarrow -\mathbf{c}$ ($i = 3$), $\mathbf{b} \rightarrow -\mathbf{b}$ ($i = 4$), and $\mathbf{T}_i \rightarrow \mathbf{T}_1$. In the S-$Pbca$ structure the tilting angle is about twice as large, while the rotation angle is slightly smaller.

action, could also lead to wrong conclusions on the origin of the transition.

In this Letter we address the problem by means of the local-density approximation (LDA) + dynamical mean-field theory (DMFT) approach [17] with a continuous-time quantum Monte Carlo (QMC) solver [18]. This method allows us to treat realistically both the material-dependence and the many-body effects. We show that the Mott transition occurs because of the L- $\rightarrow$ S-$Pbca$ structural phase transition, which is also responsible for $\sim xy$ orbital order (OO). In the metallic phases we find, with increasing x, a progressive transfer of electrons from xy to xz/yz ($p \leq 0$); down to ~ 300 K, we find, however, no orbital-selective Mott transition.

We use the *ab initio* downfolding approach based on the N-th order muffin-tin orbital (NMTO) method to construct from first-principles material-specific Wannier functions [14] which span the t_{2g} bands, and the corresponding, material-specific, three-band Hubbard model, with full local Coulomb interaction [19]

$$H = - \sum_{m,m',i,i',\sigma} t^{i,i'}_{mm'} c^{\dagger}_{im\sigma} c_{i'm'\sigma} + U\sum_{im} n_{im\uparrow} n_{im\downarrow}$$
$$+ \sum_{\substack{i\sigma\sigma' \\ m\neq m'}} (U - 2J - J\delta_{\sigma,\sigma'}) n_{im\sigma} n_{im'\sigma'}$$
$$- J \sum_{im\neq m'} [c^{\dagger}_{im\uparrow}(c^{\dagger}_{im'\uparrow}c_{im\downarrow} + c^{\dagger}_{im\downarrow}c_{im'\uparrow})c_{im'\downarrow}]. \quad (1)$$

Here $c^{\dagger}_{im\sigma}$ creates an electron with spin σ in the Wannier state m at site i, and $n_{m\sigma} = c^{\dagger}_{im\sigma}c_{im\sigma}$. The *ab initio* parameters $t^{i,i'}_{mm'}$ (Table I) are the crystal-field splittings ($i = i'$) and hopping integrals ($i \neq i'$). U and J are the direct and exchange screened Coulomb interaction. We use $U = 3.1$ eV and $J = 0.7$ eV, in line with experimental [11,20,21] and theoretical [22] estimates. The last row in (1) describes the spin-flip and pair-hopping Coulomb terms. We solve (1) by DMFT [23] with a weak-coupling continuous-time QMC [18] solver. We retain the full self-energy matrix in orbital space, $\Sigma_{m,m'}$ [14]. Our calculations yield the Green function matrix on the imaginary axis; we obtain the spectral matrix on the real axis by using a stochastic approach [24]. For limit cases (no spin-flip and pair-hopping terms) we perform comparative calculations with an alternative LDA + DMFT scheme, based on the projection of LDA Bloch states (obtained via the projector-augmented wave method [25], Vienna *Ab Initio* Simulation Package [26]) to local orbitals [27] and a Hirsch-Fye QMC solver [28]. The parameters obtained with the two methods are very similar.

The nearest-neighbor hopping integrals $t^{i,i+\mathbf{x}}_{xy,xy}$, $t^{i,i+\mathbf{x}}_{xz,xz}$, $t^{i,i+\mathbf{y}}_{xy,xy}$ progressively decrease going from the ideal tetragonal Sr$_2$RuO$_4$ (see Ref. [29]) to the L-$Pbca$ and then the S-$Pbca$ structure of Ca$_2$RuO$_4$; correspondingly, the bandwidth decreases from 2.8 eV (L-$Pbca$) to 2.5 eV (S-$Pbca$). The cause is the increase in tilting of the RuO$_6$ octahedra and deformation of the Ca cage, via Ru-O but also Ca-Ru

TABLE I. Ca$_{2-x}$Sr$_x$RuO$_4$ ($x = 0$, 0.2): hopping integrals $t^{ii'}_{m,m'}$/meV between sites $i' = 1$ and $i \sim l\mathbf{x} + m\mathbf{y} + n\mathbf{z}$, and ($x = 0$) crystal-field splitting $\Delta E_{\alpha,1}$/meV $= \varepsilon_\alpha - \varepsilon_1$ ($\alpha = 1, 2, 3$) and orbitals at site 1. Orbitals and hopping integrals for sites 2, 3, and 4 can be obtained using symmetries (Fig. 1).

L-$Pbca$ Ca$_2$RuO$_4$							
lmn	$t_{yz,yz}$	$t_{yz,xz}$	$t_{yz,xy}$	$t_{xz,yz}$	$t_{xz,xz}$	$t_{xz,xy}$	$t_{xy,xy}$
100	10	-88	-6	75	242	-50	230
010	242	-88	-35	75	10	26	230

$$\Delta E_{\alpha,1} = \begin{pmatrix} 0 \\ 103 \\ 121 \end{pmatrix}, \begin{pmatrix} |1\rangle \\ |2\rangle \\ |3\rangle \end{pmatrix} = \begin{pmatrix} 0.259 & 0.255 & 0.932 \\ 0.785 & -0.618 & -0.050 \\ 0.563 & 0.744 & -0.360 \end{pmatrix} \begin{pmatrix} |yz\rangle \\ |xz\rangle \\ |xy\rangle \end{pmatrix}$$

S-$Pbca$ Ca$_2$RuO$_4$							
lmn	$t_{yz,yz}$	$t_{yz,xz}$	$t_{yz,xy}$	$t_{xz,yz}$	$t_{xz,xz}$	$t_{xz,xy}$	$t_{xy,xy}$
100	11	-61	-25	38	123	-47	205
010	123	-61	-34	38	11	45	205

$$\Delta E_{\alpha,1} = \begin{pmatrix} 0 \\ 308 \\ 341 \end{pmatrix}, \begin{pmatrix} |1\rangle \\ |2\rangle \\ |3\rangle \end{pmatrix} = \begin{pmatrix} 0.246 & -0.009 & 0.969 \\ 0.420 & 0.903 & -0.098 \\ 0.874 & -0.430 & -0.227 \end{pmatrix} \begin{pmatrix} |yz\rangle \\ |xz\rangle \\ |xy\rangle \end{pmatrix}$$

L-$Pbca$ Ca$_{1.8}$Sr$_{0.2}$RuO$_4$							
lmn	$t_{yz,yz}$	$t_{yz,xz}$	$t_{yz,xy}$	$t_{xz,yz}$	$t_{xz,xz}$	$t_{xz,xy}$	$t_{xy,xy}$
100	9	-90	-6	87	275	-46	242
010	275	-90	-31	87	9	24	242

and Ca-O covalency [14]; for similar reasons [14], the crystal-field splitting increases from ~ 100 meV (L-$Pbca$) to ~ 300 meV (S-$Pbca$). The crystal-field orbitals are displayed in Fig. 2. For the L-$Pbca$ phase our LDA calculations yield $p_{\text{LDA}} \sim 0$. This may appear surprising, since at 2/3 filling due to the difference in bandwidth ($W_{xz/yz} \sim 1.5$ eV and $W_{xy} \sim 2.8$ eV) one might expect $p < 0$. Such an effect, however, is canceled by the crystal-field splitting of about 100 meV: since the lowest energy state is $|1\rangle = 0.932|xy\rangle + 0.259|yz\rangle + 0.255|xz\rangle$ (see Fig. 2 and Table I), i.e., close to $|xy\rangle$, neglecting the difference in bandwidth, the crystal-field splitting favors $p > 0$. For the S-$Pbca$ structure we find $W_{xz/yz} \sim 1.3$ eV and $W_{xy} \sim 2.5$ eV; i.e., the bandwidths decrease by about 0.2 eV. The crystal-field splitting is 300 meV, and the lowest energy crystal-field orbital, $|1\rangle$, is basically identical to $|xy\rangle$. The effect of the crystal-field is stronger than in the L-$Pbca$ structure leading to $p_{\text{LDA}} \sim 0.37$.

The LDA + DMFT solution of Hamiltonian (1) yields the following results: for the L-$Pbca$ structure we find a metallic solution down to very low temperatures; the orbital polarization is $p \sim 0$ at 390 K, i.e., close to the LDA value. The self-energy (Fig. 3) exhibits a narrow Fermi-liquid regime with kinks [30]; a (lower) estimate of the effective masses of the quasiparticles, obtained from the slope of Im$\Sigma_{m,m}(i\omega_n)$ at the first Matsubara frequency, is $m^*/m \sim 5.0$ (xy) and $m^*/m \sim 4.2$ (xz, yz). We find similar
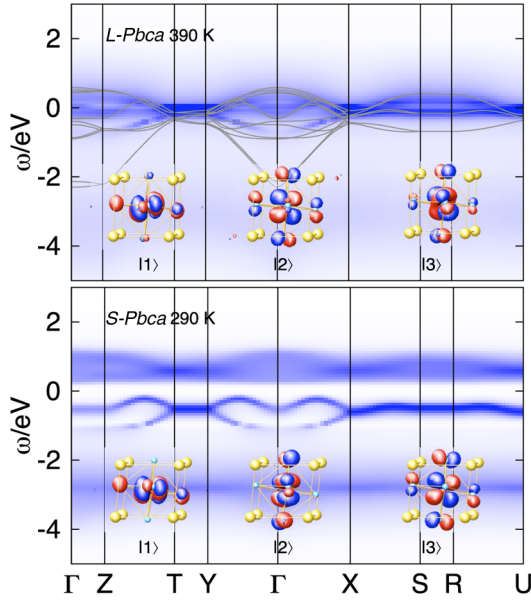
FIG. 2 (color online). The Mott transition: correlated bands for *L*- (top) and *S-Pbca* (bottom), LDA bands (*L-Pbca*, solid lines), and crystal-field orbitals for site 1 (see Table I). Positive (negative) lobes are light (dark). *S-Pbca*: $|1\rangle$ is full, $|2\rangle$ and $|3\rangle$ half-filled; the valence band has character $|1\rangle$.

behavior in Sr_2RuO_4; in Ca_2RuO_4 the mass enhancement is larger, because of the narrower bandwidth. Lowering the temperature down to 290 K turns the system into a ferromagnet with (almost) half-metallic behavior and $p \sim -0.05$ (the occupation of $|xy\rangle$ slightly decreases). The correlated bands for Ca_2RuO_4 are shown in Fig. 2. Along ΓX we find dispersive bands, while along XS the bands become almost flat.

For the *S-Pbca* structure the situation is completely different. We find a MIT between 390 and 290 K, in very good agreement with the experimental 360 K [1]. At 580 K the spectral function exhibits a pseudogap; $n_{xy} \sim 1.9$ and $n_{xz/yz} \sim 1.1$, and the polarization is already as large as $p \sim 0.8$. At 290 K the gap is open and about 0.2 eV wide (see Fig. 3), while $p \sim 1$. The most occupied state is basically identical to the LDA lowest energy crystal-field orbital (Table I); the orbital order is close to xy ferro-order, with a small antiferro component. LDA + U calculations for the antiferromagnetic phase yield an OO consistent with our results for the paramagnetic phase [5,6]. Such orbital order in the *S-Pbca* phase and none in the *L-Pbca* phase is in line with the evolution, across the MIT, of the O 1s x-ray absorption (XAS) spectra [11,12] with increasing light incidence angle, θ. Our spectral functions are also consistent with photoemission [12,31]: the quasiparticle peak in the high-temperature phase, the Hubbard band at -0.5 eV, and the multiplets at -3 eV all correspond to features in the experimental spectra. The experimental peak centered at ~ -1.5 eV in [12,31], absent in our t_{2g} spectral functions, likely includes a sizable contribution of the O bands,

which start around those energies. The small gap (*S-Pbca*) is in excellent agreement with electrical resistivity [1,4] and optical conductivity [10] data.

In Fig. 3 we investigate the role played by the spin-flip and pair-hopping Coulomb terms by comparing results with and without those terms. We find that the effective masses decrease when the full Coulomb interaction is considered; this happens because the average U decreases and the degeneracy of the low energy d^3 and d^4 multiplets increases. In the insulating phase, such a difference in multiplet degeneracy appears very clearly as the enhancement of the $d^4 \rightarrow d^3$ peak around ~ -0.5 eV. The differences in orbital polarization are small.

Our results show that the Mott transition in Ca_2RuO_4 is driven by the $L \rightarrow S$-*Pbca* structural transition at T_S and occurs simultaneously with orbital order. For the *L-Pbca* structure we find no OO for temperatures well below T_S; OO follows, rather than produces, the change in structure [32]. These findings are in very good agreement with resonant x-rays scattering interference data [9], which show that the xy OO disappears close to the the MIT. They are also in line with the fact that a tiny pressure (~ 0.5 GPa) is sufficient to make the system metallic at 290 K via the *S*- to *L-Pbca* transition [2].

Can this scenario be extended to $Ca_{2-x}Sr_xRuO_4$ ($x \leq 0.2$)? Let us examine the limit system $x = 0.2$, for which the *L-Pbca* phase persists down to 10 K. Neglecting the chemical effects of the $Ca \rightarrow Sr$ substitution [33] and disorder effects, for the 10 K structure we find crystal-field splittings of 81 and 110 meV, slightly (~ 0.1 eV) broader t_{2g} bands than for $x = 0$, and $p_{LDA} \sim -0.03$. The main difference with the *L-Pbca* structure of Ca_2RuO_4 is in the crystal-field orbitals (e.g., $\langle xy|1\rangle \sim \langle xy|2\rangle \sim 0.66$), and can be ascribed to the differences in octahedra tilting and rotation, and corresponding distortions of the cation cage. All of these effects stabilize the metallic solution. With LDA + DMFT (390–290 K) we find three metallic bands, in line with ARPES results from Ref. [8], with $m^*/m \sim 3.7$ (xz), 4.4 (yz), 5.6 (xy); $p \sim -0.14$. While the details slightly differ, depending on x [34], we conclude that for $x \leq 0.2$ the temperature-induced Mott transition is mostly driven by the change in structure *L-Pbca* $\rightarrow$ *S-Pbca*. We find no OSMT down to 290 K.

What happens for $x > 0.2$? For the $x = 0.5$ structure [33] the crystal-field states are $|1\rangle = |xy\rangle$, and $|xz\rangle$, $|yz\rangle$, the crystal-field splitting is small, $p_{LDA} = -0.02$, $W_{xy} \sim 2.7$ eV, $W_{xz/yz} \sim 1.6$ eV. LDA + DMFT at 390 K yields again a metallic solution with $m^*/m \sim 4.0$ (xz/yz) and 5.6 (xy), and three metallic bands, in agreement with ARPES [35]; $p \sim -0.15$ at 390–290 K.

Thus, outside the *S-Pbca* phase we always find a metal, in line with transport and optical conductivity data [3,4,36]; with increasing x, $n_{xz} + n_{yz}$ increases, in line with XAS [37]; $p \sim 0$ or slightly negative, approaching the $p = -1/2$ of the OSMT scenario [5]; we find, however, no OSMT down to 290 K.
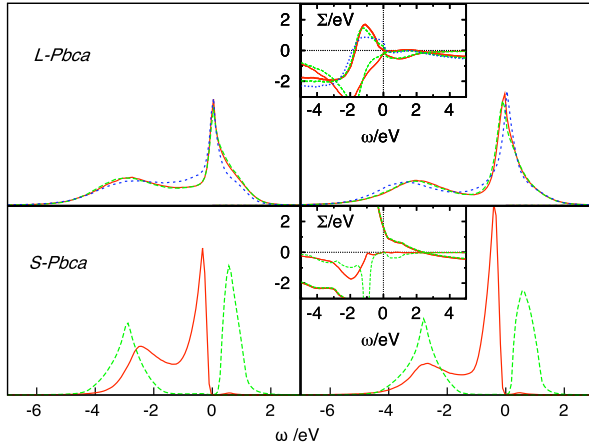
FIG. 3 (color online). Spectral matrix. Solid lines: $A_{1,1}$. Dashed lines: $A_{2,2}$ and $A_{3,3}$. Left: density-density terms only. Right: rotationally invariant Coulomb vertex. First row: L-$Pbca$, $T = 390$ K. Second row: S-$Pbca$, $T = 290$ K. Inset: Real (thick lines) and imaginary (thin lines) self-energies.

In conclusion, we have studied the origin of the metal-insulator transition in Ca_2RuO_4. We find that it is driven by the structural L- $\to$ S-$Pbca$ transition. Two mechanisms compete; while a small $W_{xz/yz}/W_{xy}$ bandwidth ratio enhances the occupation of the xz/yz orbitals ($p < 0$) and could lead to an orbital-selective Mott transition with $p = -1/2$ [5], a large crystal-field splitting $\Delta_{3,1}$, with $|1\rangle \sim |xy\rangle$ as the lowest energy state, favors xy orbital order and $p > 0$, as in Ref. [13]. In the $x = 0$ L-$Pbca$ structure the two effects compensate: $\Delta_{3,1}/W_{xy} \sim 0.04$, $\langle 1|xy\rangle \sim 0.93$, and $W_{xz/yz}/W_{xy} \sim 0.54$. We find a metallic solution above and well below $T_{MIT} \sim 360$ K, with orbital polarization $p \sim 0$ (no orbital order) at $T \sim 390$ K. At low temperatures the system becomes a ferromagnetic metal, in line with (moderate) pressure studies [2]. In the $x = 0$ S-$Pbca$ structure $\Delta_{3,1}/W_{xy} \sim 0.13$, sizably larger than for the L-$Pbca$ structure, $\langle 1|xy\rangle \sim 0.97$, and $W_{xz/yz}/W_{xy} \sim 0.52$; the system becomes insulating around T_{MIT} and $p \sim 1$ ($\sim xy$ ferro-orbital order), in excellent agreement with experiments; orbital order follows, rather than drives, the transition. Our results indicate that this scenario can be extended to $Ca_{2-x}Sr_xRuO_4$ for all $x \le 0.2$. Finally, for the metallic $x \le 0.5$ phases we find that, differently than in the crystal-field scenario [13], $p \sim 0$ or negative, slowly approaching the $-1/2$ of Ref. [5] with increasing x, but, down to ~ 300 K, we find no orbital-selective Mott transition.

Calculations were performed on the Jülich BlueGene/P. We thank A. Hendricks, T. Koethe, and H. Tjeng for sharing with us their data before publication.

[1] C. S. Alexander *et al.*, Phys. Rev. B **60**, R8422 (1999).
[2] F. Nakamura *et al.*, Phys. Rev. B **65**, 220402(R) (2002); P. Steffens *et al.*, Phys. Rev. B **72**, 094104 (2005).
[3] O. Friedt *et al.*, Phys. Rev. B **63**, 174432 (2001).
[4] S. Nakatsuji and Y. Maeno, Phys. Rev. Lett. **84**, 2666 (2000); Phys. Rev. B **62**, 6458 (2000).
[5] V. I. Anisimov *et al.*, Eur. Phys. J. B **25**, 191 (2002).
[6] Z. Fang, N. Nagaosa, and K. Terakura, Phys. Rev. B **69**, 045116 (2004); New J. Phys. **7**, 66 (2005).
[7] M. Neupane *et al.*, Phys. Rev. Lett. **103**, 097001 (2009).
[8] A. Shimoyamada *et al.*, Phys. Rev. Lett. **102**, 086401 (2009).
[9] M. Kubota *et al.*, Phys. Rev. Lett. **95**, 026401 (2005); I. Zegkinoglou *et al.*, Phys. Rev. Lett. **95**, 136401 (2005).
[10] A. V. Puchkov *et al.*, Phys. Rev. Lett. **81**, 2747 (1998).
[11] T. Mizokawa *et al.*, Phys. Rev. B **69**, 132410 (2004).
[12] T. Mizokawa *et al.*, Phys. Rev. Lett. **87**, 077202 (2001).
[13] A. Liebsch and H. Ishida, Phys. Rev. Lett. **98**, 216403 (2007).
[14] E. Pavarini *et al.*, Phys. Rev. Lett. **92**, 176403 (2004); E. Pavarini, A. Yamasaki, J. Nuss, and O. K. Andersen, New J. Phys. **7**, 188 (2005).
[15] M. Braden *et al.*, Phys. Rev. B **58**, 847 (1998).
[16] P. Werner, E. Gull, M. Troyer, and A. J. Millis, Phys. Rev. Lett. **101**, 166405 (2008); P. Werner, E. Gull, and A. J. Millis, Phys. Rev. B **79**, 115119 (2009); L. de Medici *et al.*, Phys. Rev. Lett. **102**, 126401 (2009).
[17] V. I. Anisimov *et al.*, J. Phys. Condens. Matter **9**, 7359 (1997); A. I. Lichtenstein and M. I. Katsnelson, Phys. Rev. B **57**, 6884 (1998).
[18] A. N. Rubtsov, V. V. Savkin, and A. I. Lichtenstein, Phys. Rev. B **72**, 035122 (2005).
[19] J. Kanamori, Prog. Theor. Phys. **30**, 275 (1963).
[20] T. Yokoya *et al.*, Phys. Rev. B **53**, 8151 (1996).
[21] J. H. Jung *et al.*, Phys. Rev. Lett. **91**, 056403 (2003).
[22] Z. V. Pchelkina *et al.*, Phys. Rev. B **75**, 035122 (2007).
[23] A. Georges, G. Kotliar, W. Krauth, and M. J. Rozenberg, Rev. Mod. Phys. **68**, 13 (1996).
[24] A. S. Mishchenko, N. V. Prokof'ev, A. Sakamoto, and B. V. Svistunov, Phys. Rev. B **62**, 6317 (2000).
[25] P. E. Blöchl, Phys. Rev. B **50**, 17953 (1994).
[26] G. Kresse and D. Joubert, Phys. Rev. B **59**, 1758 (1999).
[27] B. Amadon *et al.*, Phys. Rev. B **77**, 205112 (2008).
[28] J. E. Hirsch and R. M. Fye, Phys. Rev. Lett. **56**, 2521 (1986).
[29] E. Pavarini and I. I. Mazin, Phys. Rev. B **74**, 035115 (2006).
[30] K. Byczuk *et al.*, Nature Phys. **3**, 168 (2007).
[31] A. Hendricks, T. Koethe, and H. Tjeng (unpublished).
[32] E. Pavarini, E. Koch, and A. I. Lichtenstein, Phys. Rev. Lett. **101**, 266405 (2008).
[33] The effect of the full substitution Ca $\to$ Sr is the following: for $x = 0.2$ both crystal-field splitting (76 and 147 meV) and t_{2g} bandwidth increase slightly, $\langle 1|xy\rangle \sim 0.89$, $p_{LDA} \sim 0.16$. For $x = 0.5$ the crystal-field splitting increases to ~ 80 meV, with $|1\rangle = |xy\rangle$, and $p_{LDA} = 0.25$.
[34] For $x = 0.1$ LDA + DMFT (projection scheme) yields a metal for L-$Pbca$ ($p \sim 0.03$ at 580 K) and a deep pseudogap for S-$Pbca$ ($p \sim 0.85$ at 390 K). For $x = 0.15$ (L-$Pbca$) we find a metal at 390 K with $p \sim -0.07$.
[35] S.-C. Wang *et al.*, Phys. Rev. Lett. **93**, 177007 (2004).
[36] J. S. Lee *et al.*, Phys. Rev. Lett. **89**, 257402 (2002).
[37] H-J. Noh *et al.*, Phys. Rev. B **72**, 052411 (2005).